Supporting Information

Table S1: FPLC columns used for protein purification.

Sample	1st column	2nd column	3rd column
6His.LigIII$_{170-755}$	HisTrap HP	Superdex200 16/60	-
6His.Flag-TDP1	HisTrap HP	Superdex200 16/60	-
6His.LigIIIα-Flag-TDP1	HisTrap HP	HiTrap Q	Superdex200 16/60
6His.LigIII$_{170-755}$-Flag-TDP1	HisTrap HP	HiTrap SP	Superdex200 16/60
LigIIIα-6His-XRCC1	HisTrap HP	Superdex200 16/60	HiTrap Q
Strep-LigIIIα-6His-XRCC1-TDP1	HisTrap HP	Superdex200 16/60	HiTrap Q

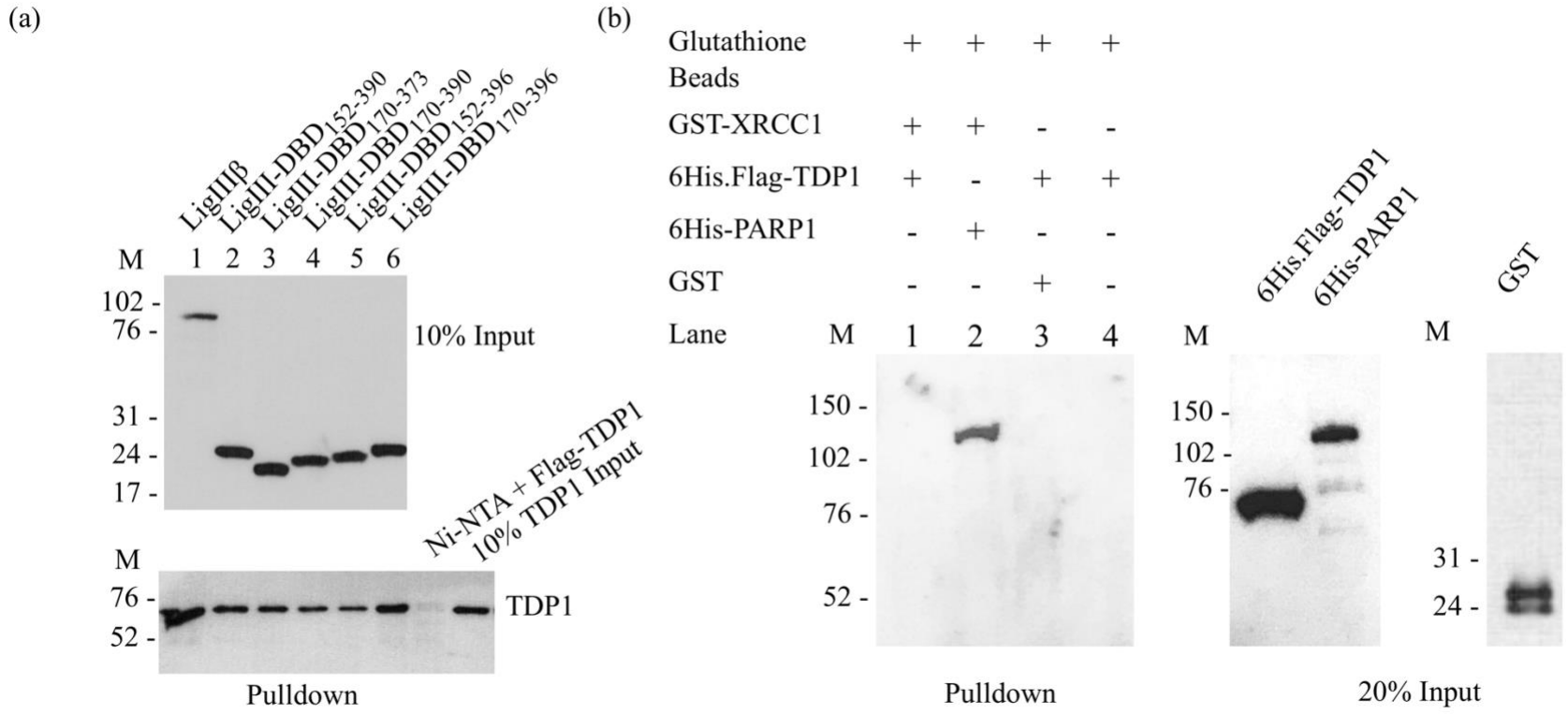

Figure S1: TDP1 interacts with different versions of LigIII-DBD but not with XRCC1 (a) Upper panel, 10% input of LigIIIβ, LigIII-DBD$_{152-390}$, LigIII-DBD$_{170-373}$, LigIII-DBD$_{170-390}$, LigIII-DBD$_{152-396}$, LigIII-DBD$_{170-396}$, respectively (Lane 1-6). Immunoblotting with mouse anti-6His mAb (Abcam). Lower panel, binding of Flag-TDP1 (10 pmol) to Ni-beads liganded by full length LigIIIβ and five different DBD domains (10 pmol of each). Ni-beads alone with Flag-TDP1 is the control lane along with 10% Flag-TDP1 input. Immunoblotting with mouse anti-Flag M2 (Sigma Aldrich). **(b)** Left panel, binding of TDP1 and PARP1 (10 pmol of each) to Glutathione-S-transferase beads liganded by GST-XRCC1 (10 pmol) (lanes 1 and 2). Lanes 3 and 4 represent controls with beads liganded by GST + 6His.Flag-TDP1 and beads alone + 6His-Flag-TDP1, respectively.

Immunoblotting with mouse anti-6His mAb (Abcam) Middle panel, 10% input of 6His.Flag-TDP1, 6His-PARP1, and GST (Right panel). Immunoblotting with mouse anti-6His (Abcam) and anti-GST (Santa Cruz Biotechnology)

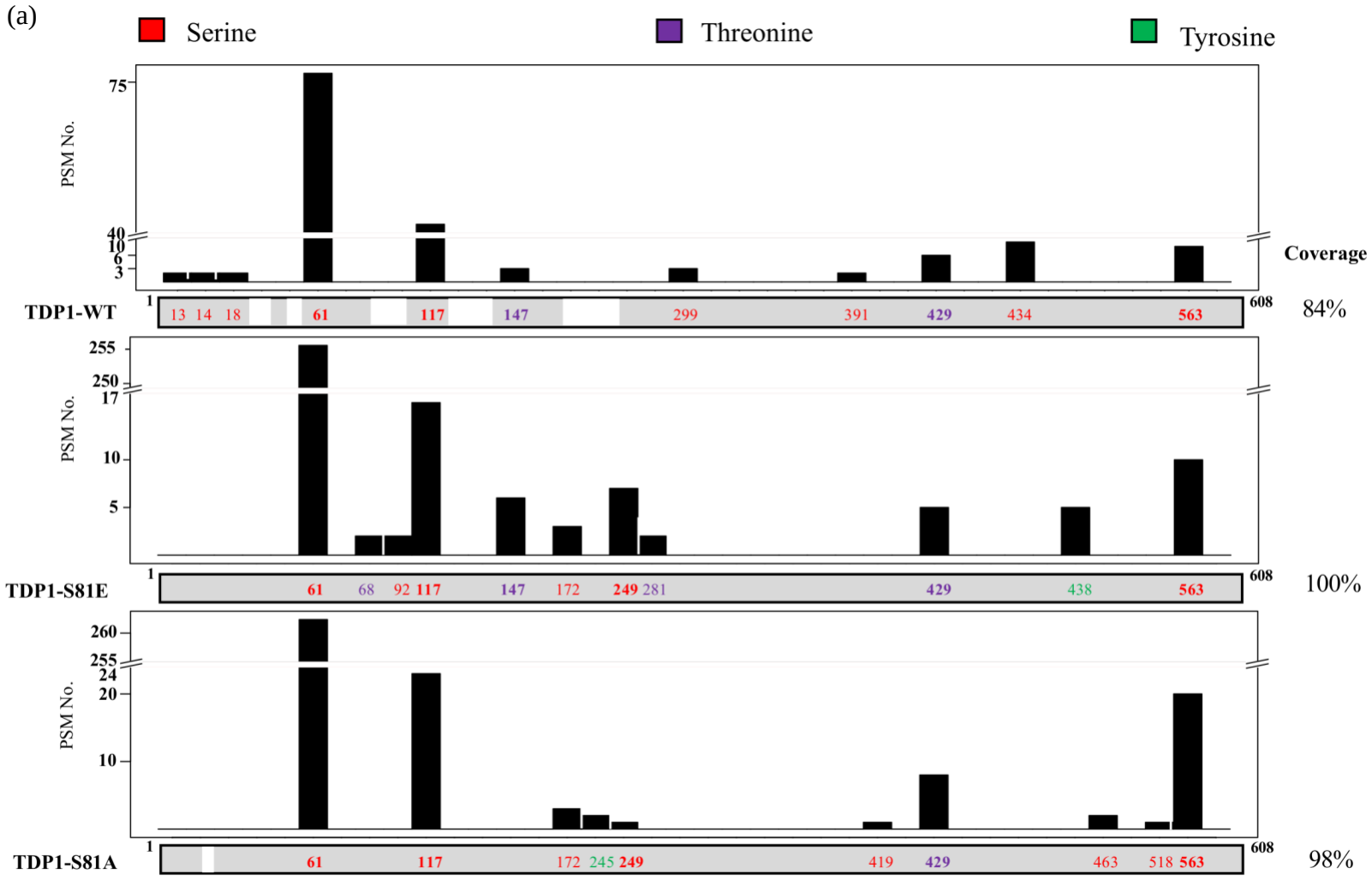

(b)

[K].FFAGSQEPMATFPVPYDLPPELYGSK.[D]

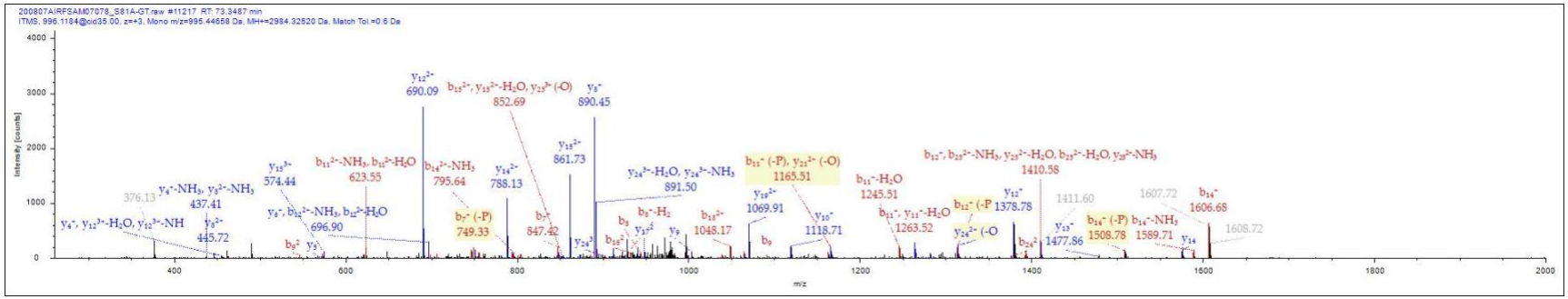

[R].TSLEGYPAGGSLPYSIQTAEK.[Q]

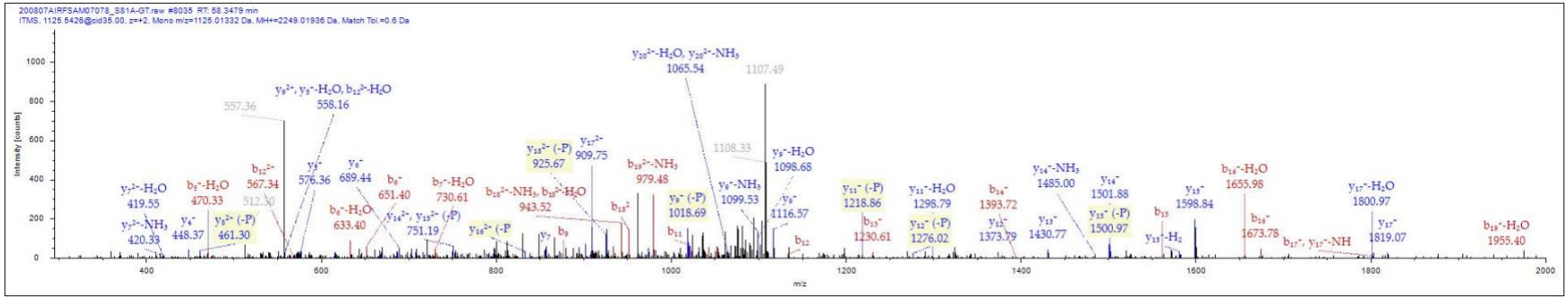

[K].AHLHAQAKPYENI**S**LCQAK.[L]

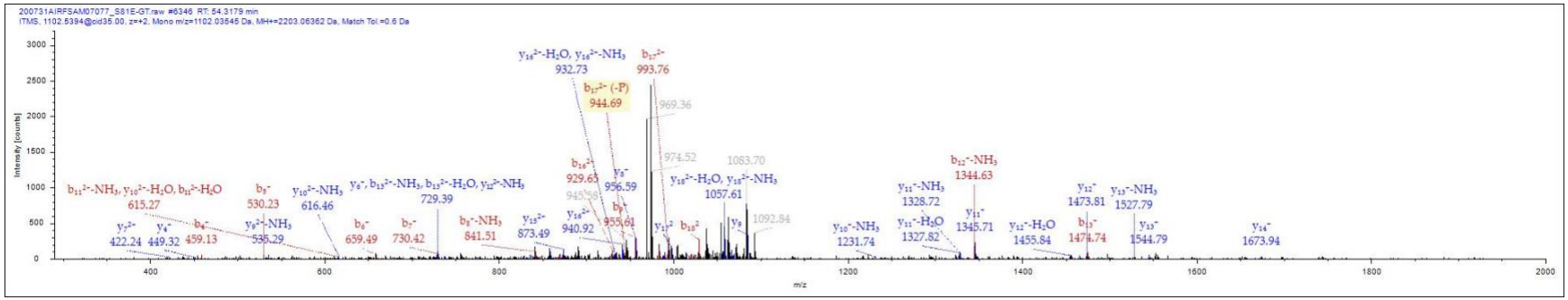

[R].LKEEEDEYE**T**SGEGQDIWDMLDK.[G]

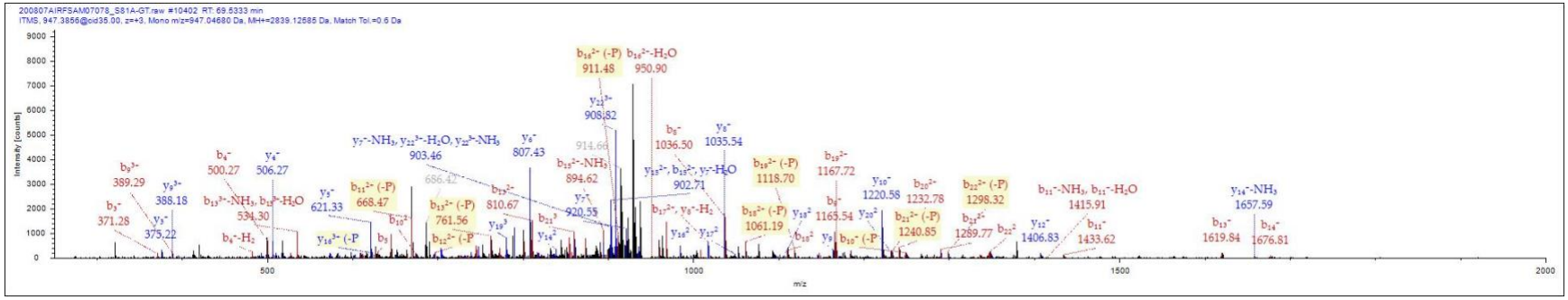

[K].IAWFLVTSANLSK.[A]

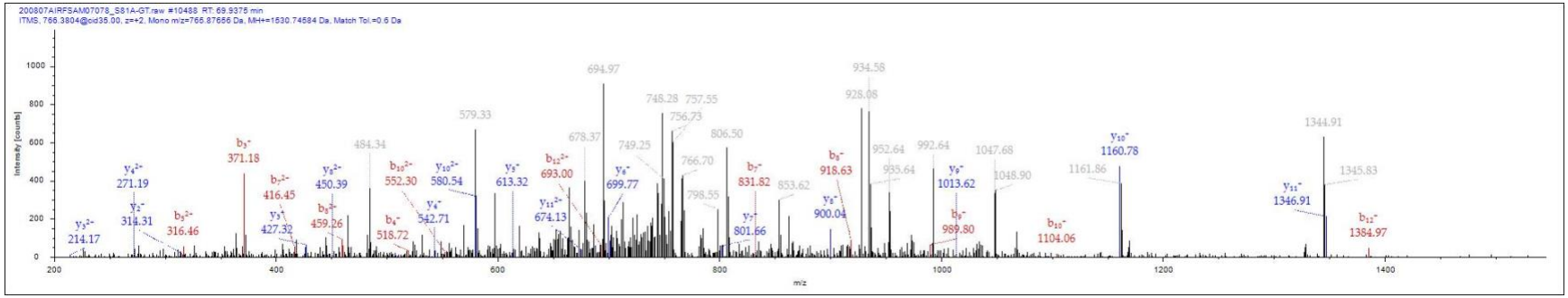

[K].WLCSEFKESMLTLGK.[E]

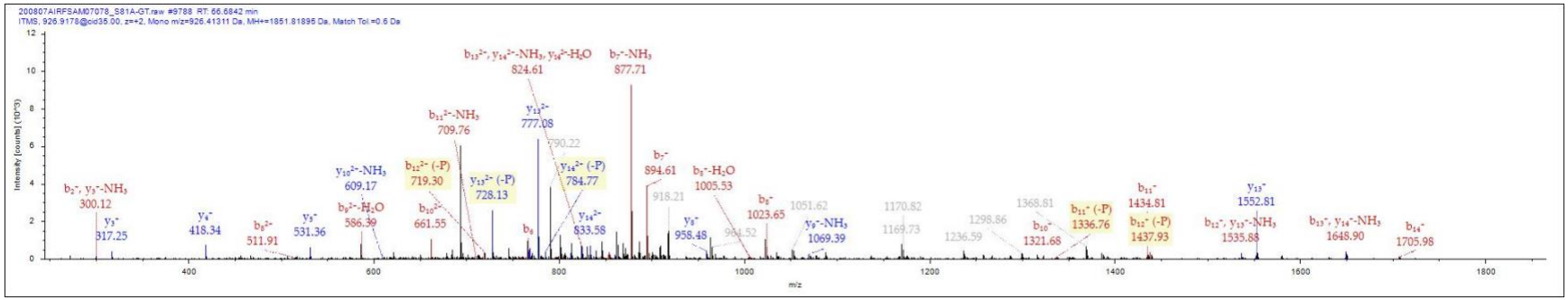

[K].KEKDI**S**APNDGTAQR.[T]

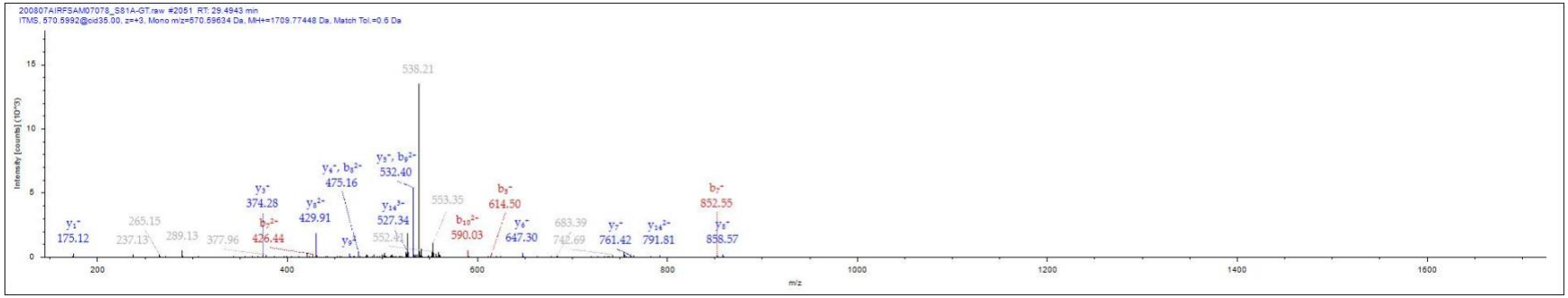

[K].I**S**PVKFSNTDSVLPPKR.[Q]

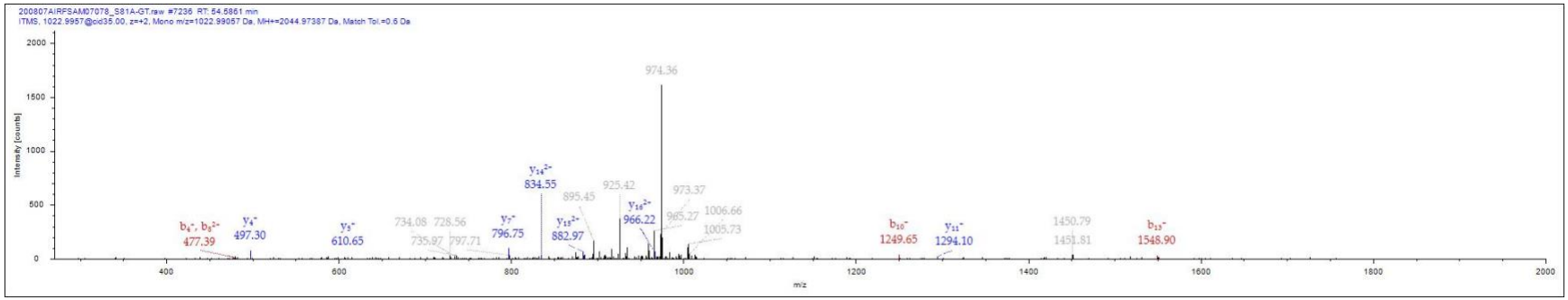

[K].RKISPVK.[F]

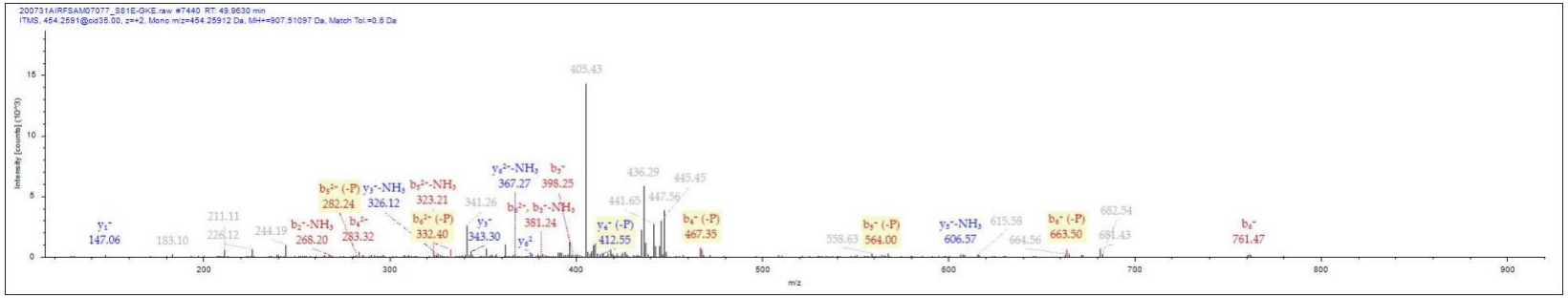

[K].GNPFQFYLTRVSGVKPK.[Y]

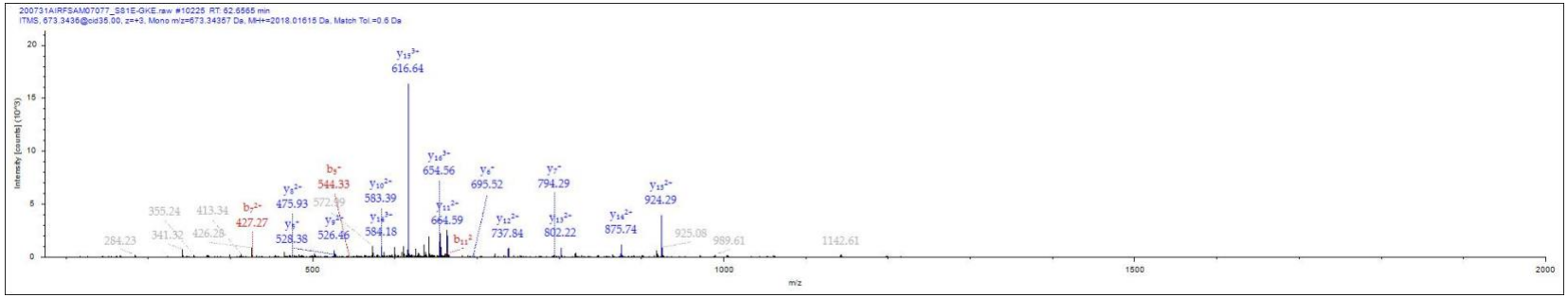

[K].DISAPNDGTAQRTE.[N]

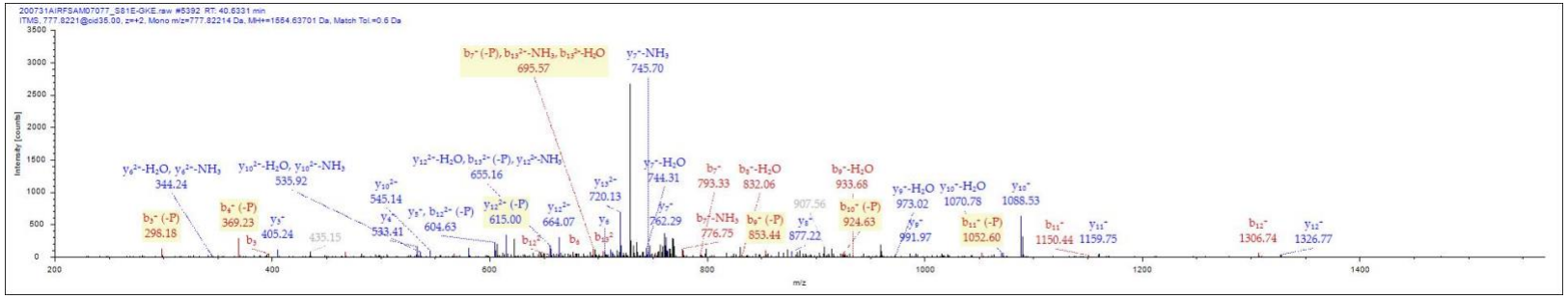

[R].KISPVKFSNTDSVLPPK.[R]

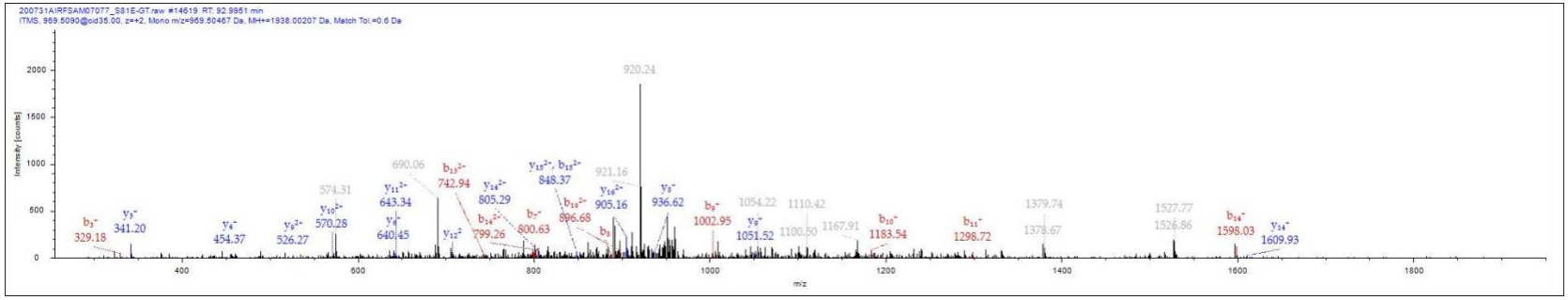

[R].VVIHTSNLIHADWHQK.[T]

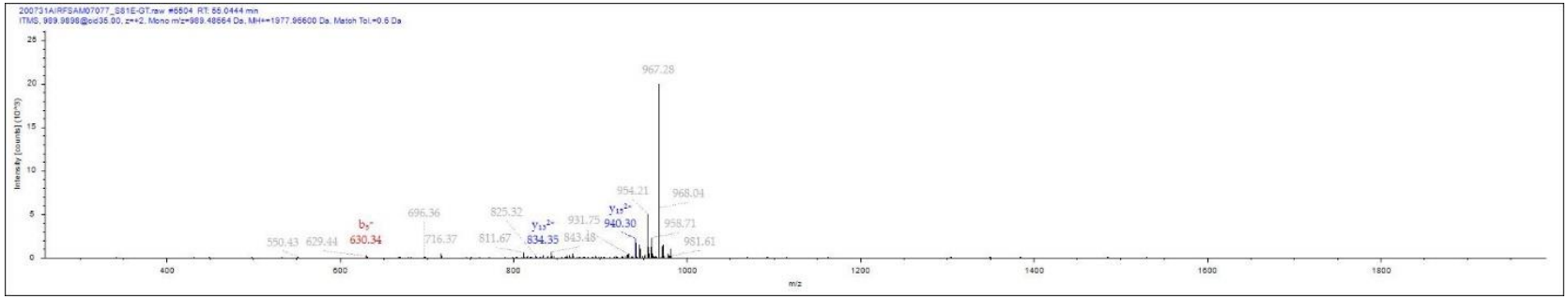

[K].TPGKSSVPLYLIYPSVENVR.[T]

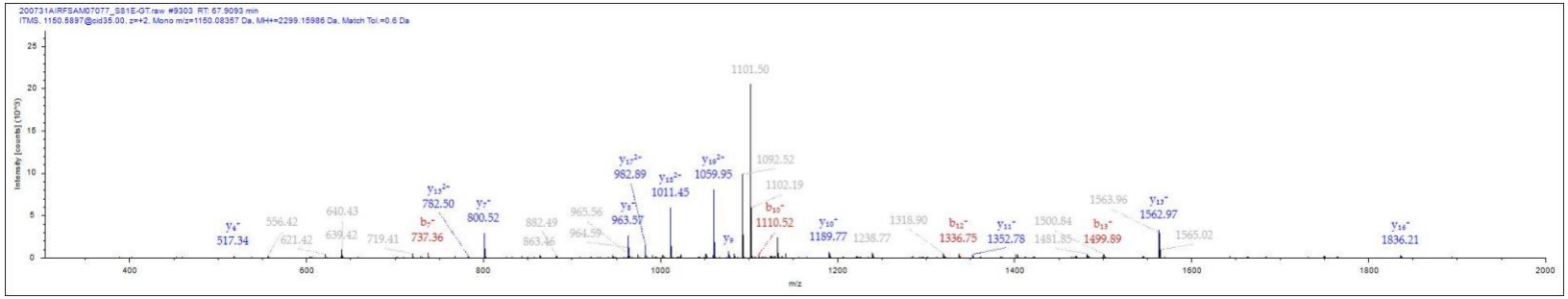

[K].ESKTPGKSSVPLYLIYPSVENVR.[T]

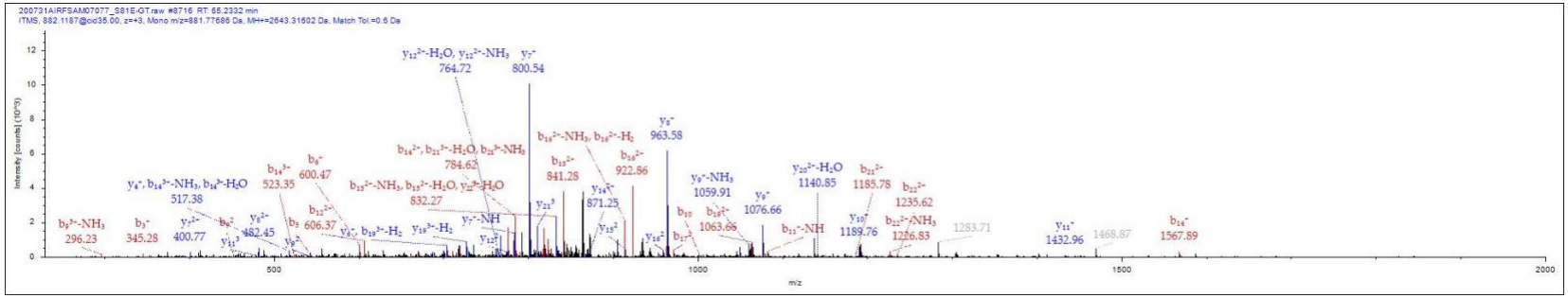

[K].EKDISAPNDGTAQR.[T]

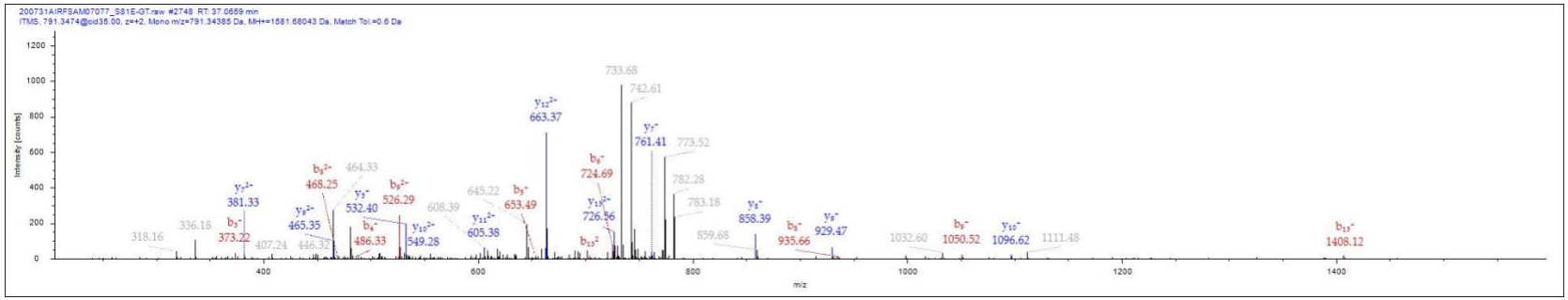

[K].ESMLTLGKESKTPGK.[S]

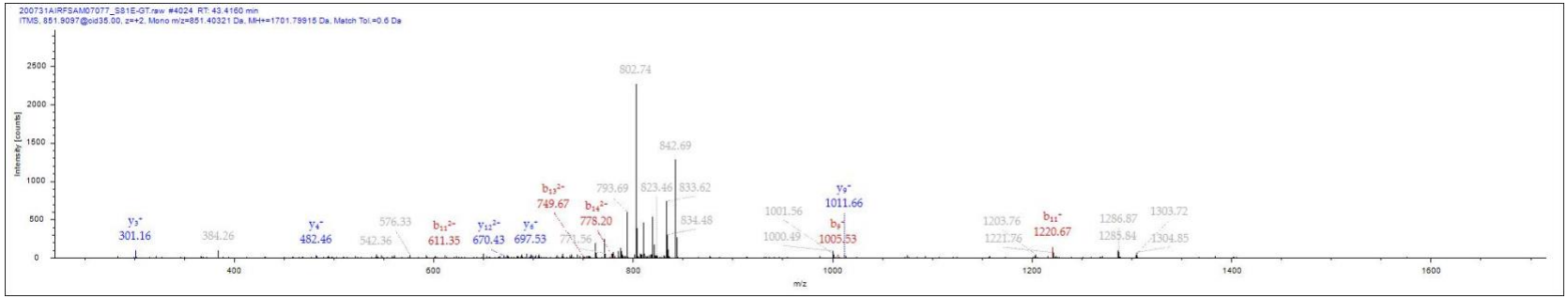

[K].SGAQEDLGWCLSSSDDELQPEMPQK.[Q]

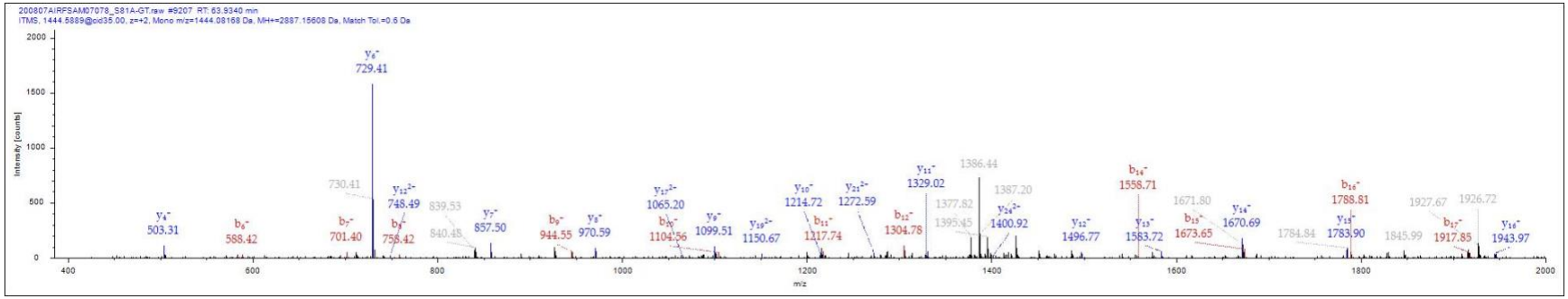

[K].SGEQEDLGWCLSSSDDELQPEMPQK.[Q]

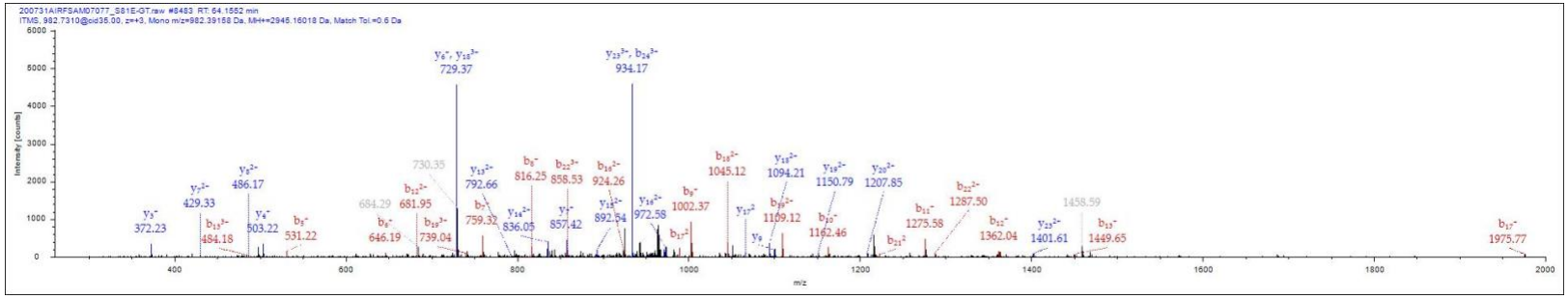

Figure S2: Identification and comparison of phosphorylated sites in insect cell-expressed TDP1 variants (WT, S81E and S81A) by mass spectrometry. **(a)** Bar diagram representing peptide spectrum matches (PSM) of TDP1-WT (top), TDP1-S81E (middle) and TDP1-S81A (bottom) at different amino acid positions. PSM indicates the total number of times the phosphorylated peptide was identified. Bold number indicating modified amino acid residues identified in more than one TDP1 variant. Modified residues were detected with 84-100% coverage of the protein sequences. **(b)** Peptide spectra detected via mass spectrometry post-translational modification studies. The phosphorylated residue is indicated in red. The last two peptides spectra represents the peptides containing the amino acid substitutions at S81 (S81>S81A and S81S>S81E) indicated in blue.

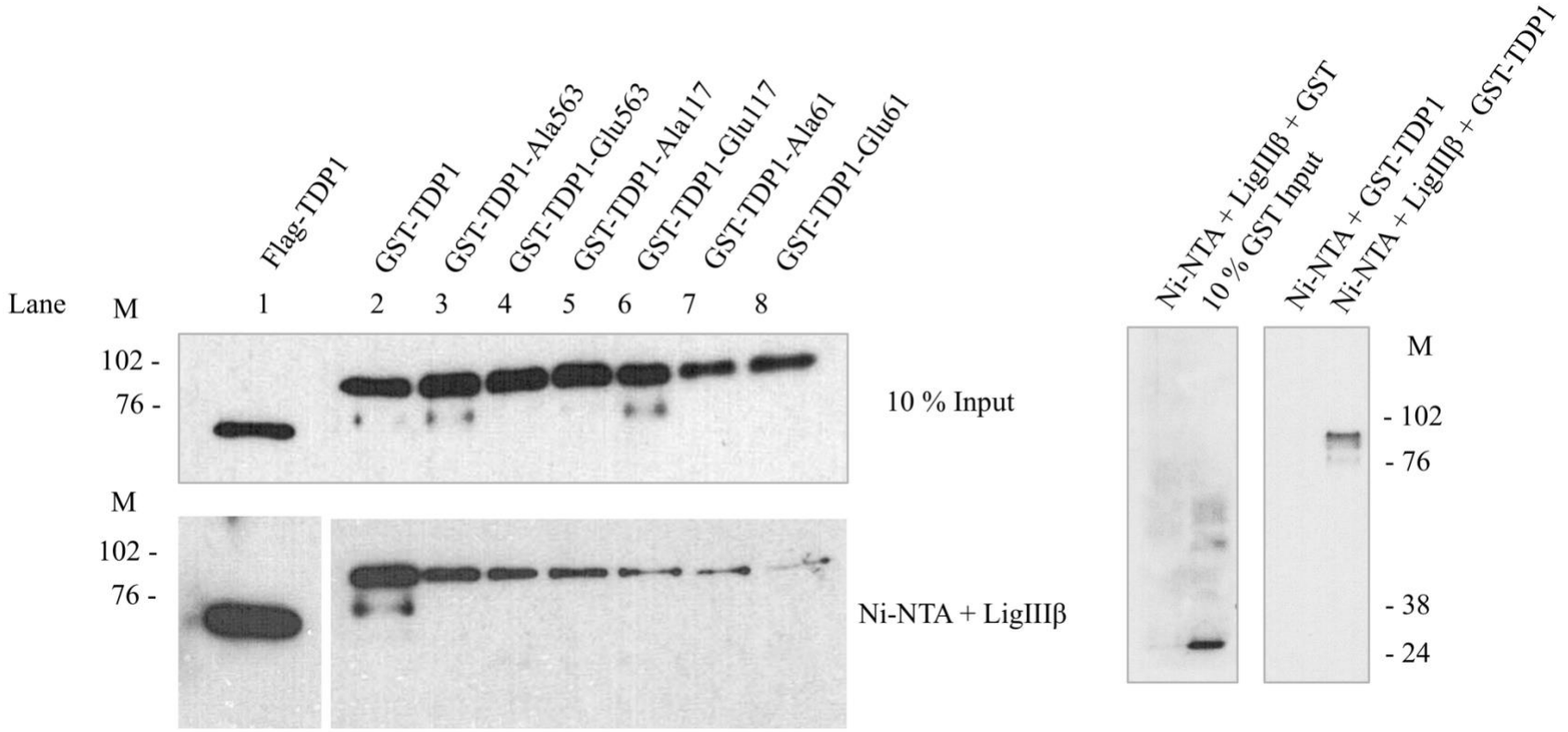

Figure S3: Single amino acid changes within the TDP1 N-terminal region reduce binding with LigIII. Upper panel (left), 10% input of insect cell synthesized TDP1 (Flag-TDP1), bacteria synthesized full length GST-TDP1, GST-TDP1-S563A, GST-TDP1-S563E, GST-TDP1-S117A, GST-TDP1-S117E, GST-TDP1-S61A, and GST-TDP1-S61E, lanes 1-8 respectively. Immunoblotting with rabbit anti-TDP1-C-term pAb (Abcam) Bottom panel (left), binding of wild type (bacteria and insect cell synthesized) and single amino acid mutants (bacteria) TDP1 to Ni-beads liganded by full-length LigIIIβ (10 pmol of each). Right panels, control blots showing Ni-beads liganded by LigIIIβ + GST (GST negative control), Ni-beads alone + GST-TDP1 (negative control), Ni-beads liganded by LigIIIβ + GST-TDP1 (positive control), and 10% GST input control. Immunoblotting with rabbit anti-GST pAb (Abcam).

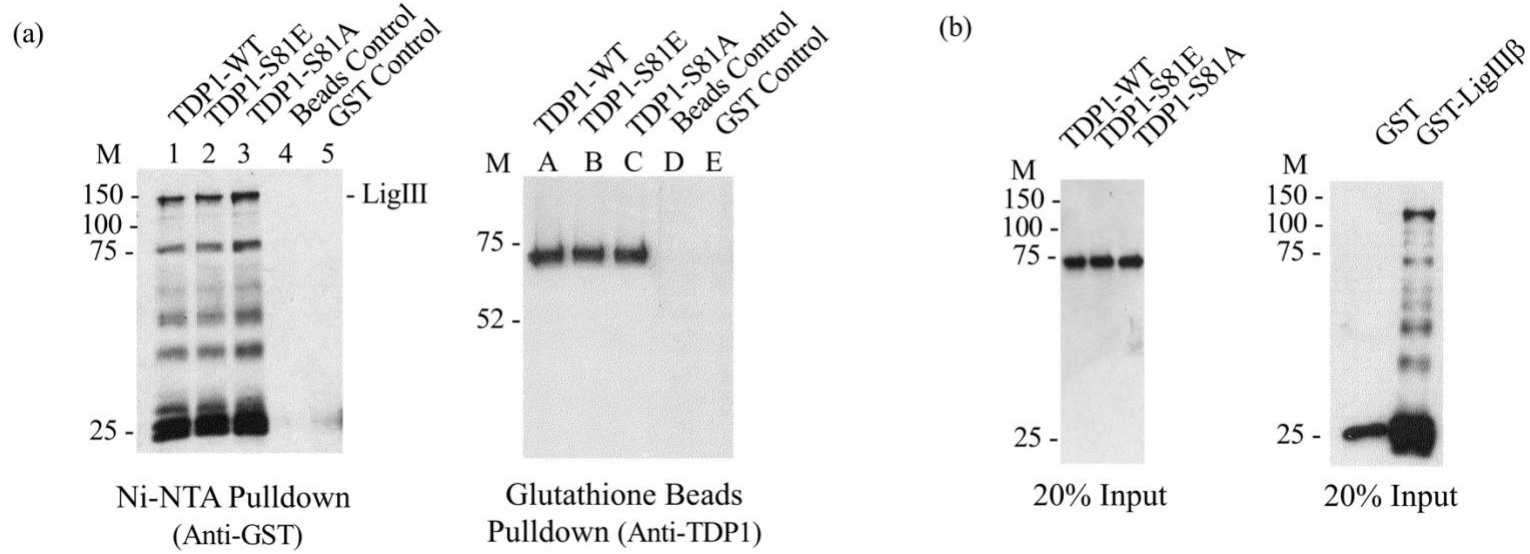

Figure S4: Similar binding of insect cell-expressed versions of TDP1 with substitutions of Ser81 with DNA LigIII. (a) Left panel, binding of GST-LigIIIβ (10 pmol) to Ni-beads liganded by 6His-Flag-TDP1 (WT, S81E and S81A) (Lane 1-3) (10 pmol of each). Lanes 4 and 5 represent controls with Ni-beads alone + GST-LigIIIβ (negative control) and Ni-beads alone + GST (GST negative control), respectively. Immunoblotting with mouse anti-GST mAb (Santa Cruz Biotechnology). Right panel, binding of GST-LigIIIβ (10 pmol) to glutathione S-transferase bead liganded by TDP1-WT, TDP1-S81E and TDP1-S81A (lane A-C, 10 pmol of each). Lanes D and E represent controls with glutathione S-transferase beads alone + TDP1-WT (negative control) and glutathione S-transferase beads liganded by GST + TDP1-WT (GST negative control), respectively. Immunoblotting with mouse anti-TDP1 mAb (Santa Cruz Biotechnology). (b) Left panel, 20% input of TDP1-WT, TDP1-S81E, TDP1-S81A and (right panel) 20% input of GST and GST-LigIIIβ. Immunoblotting with mouse anti-TDP1 mAb (Santa Cruz Biotechnology) and mouse anti-GST mAb (Santa Cruz Biotechnology).

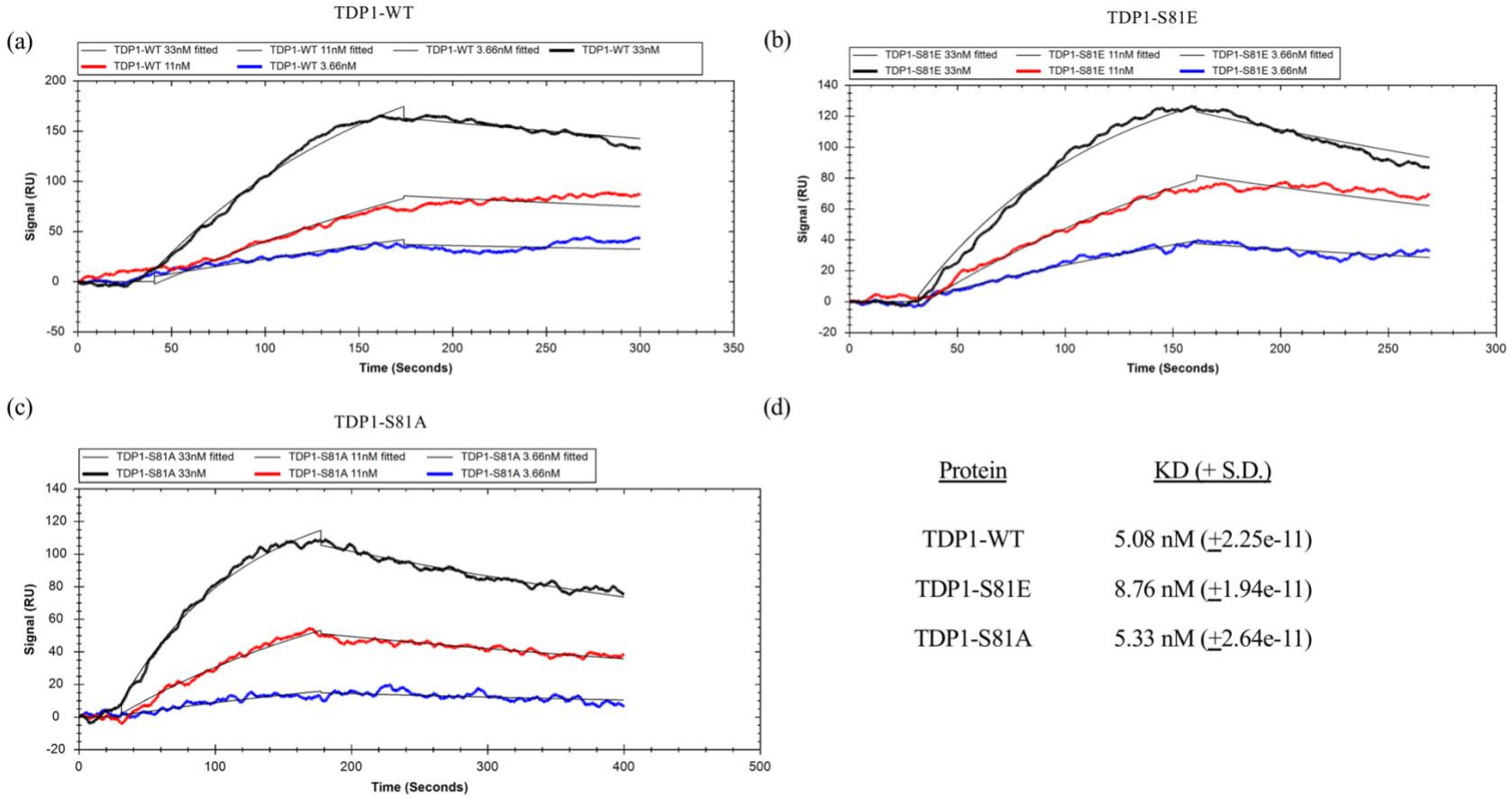

Figure S5: Kinetic analysis of TDP1 (WT, S81E and S81A) binding to LigIII. Representative sensorgrams of Flag-tagged TDP1 variants; panel **a**, WT; panel **b**, S81E and panel **c**, S81A binding to COOH sensor with LigIII. For each analyte sample, three different concentrations (3.66 nM, 11 nM and 33 nM) were injected and analyzed. (**d**) Kinetic (KD) analysis of the three TDP1 variants with the standard deviation (S.D.) using TraceDrawer software.

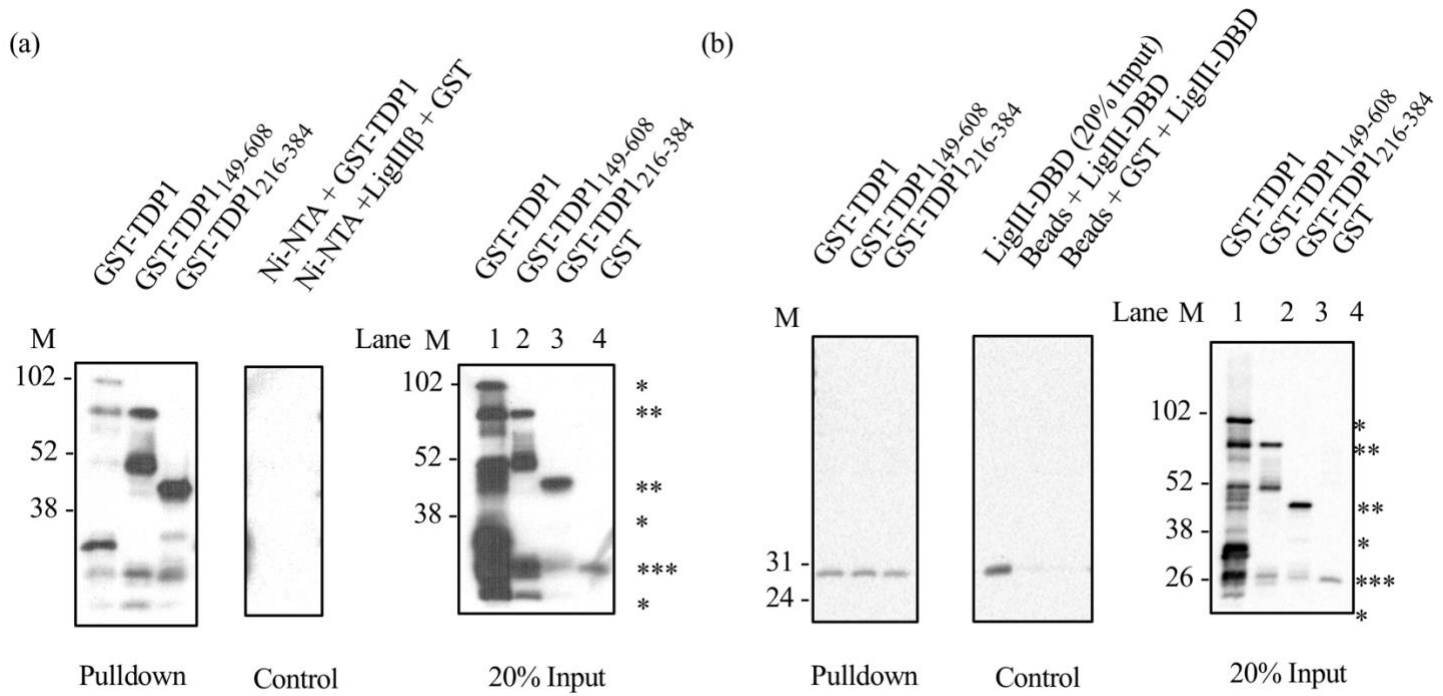

Figure S6: TDP1$_{216-384}$ interacts with full length LigIIIβ and LigIII-DBD. (a) Left panel, binding of GST-TDP1, GST-TDP1$_{149-608}$ and GST-TDP1$_{216-384}$ to (10 pmol of each) to Ni-beads liganded by full length LigIIIβ (10 pmol). Immunoblotting with rabbit anti-GST pAb (Abcam). Middle panel, control lanes with Ni-beads alone + GST-TDP1 (negative control) and Ni-beads liganded by LigIIIβ + GST (GST control). Right panel, 20% input of GST-TDP1, GST-TDP1$_{149-608}$, GST-TDP1$_{216-384}$ and GST. Immunoblotting with rabbit anti-GST mAb (Abcam). **(b)** Left panel, binding of LigIII-DBD (10 pmol) to glutathione S-transferase beads liganded by GST-tagged TDP1, GST-TDP1$_{149-608}$ and GST-TDP1$_{216-384}$ (10 pmol of each). Immunoblotting with mouse anti-6His mAb (Abcam). Middle panel, 20% input of LigIII-DBD, glutathione S-transferase beads only + LigIII-DBD (negative control) and glutathione S-transferase beads liganded by GST + LigIII-DBD (GST negative control.) Immunoblotting with mouse anti-GST mAb (Santa Cruz Biotechnology). Right panel, 20% input of GST-TDP1, GST-TDP1$_{149-608}$, GST-TDP1$_{216-384}$ and GST. Immunoblotting with mouse anti-GST mAb (Santa Cruz Biotechnology). ***** represents the band for the protein of interest.

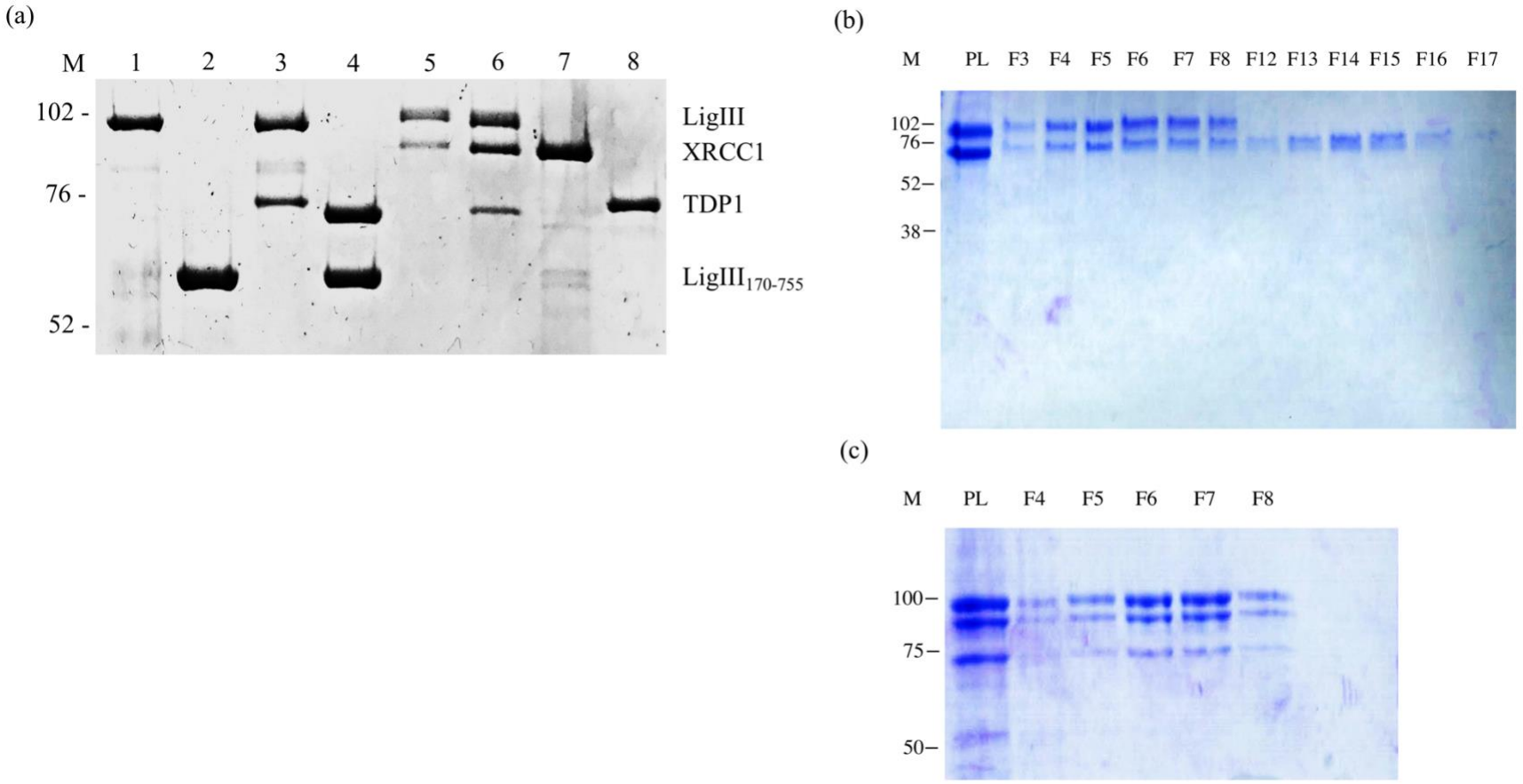

Figure S7: Purified DNA LigIII associated protein and protein complexes. **(a)** Lanes 1-8 represent LigIIIβ, LigIII$_{170-755}$, LigIIIα-TDP1, LigIII$_{170-755}$-TDP1, LigIIIα-XRCC1, LigIIIα-XRCC1-TDP1, XRCC1 and TDP1, proteins and protein complexes, respectively. All proteins were purified after expression in insect cells except for LigIIIβ. **(b)** Purification and complex formation by LigIIIα and TDP1. Major peak fractions were

run in an SDS-PAGE gel for verifying the complex formation. **(c)** Purification and complex formation by LigIIIα, TDP1 and XRCC1. Major peak fractions were run in an SDS-PAGE gel for verifying complex formation.

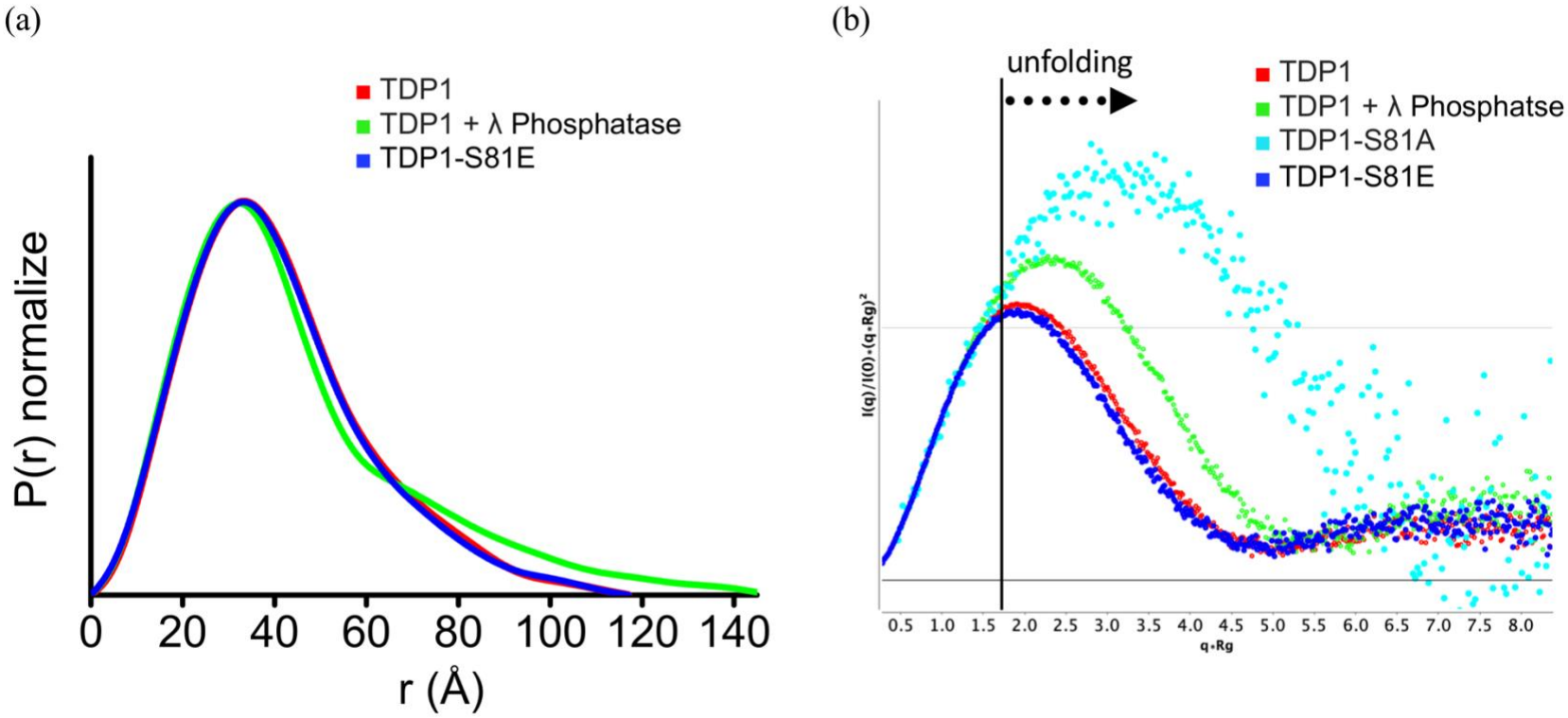

Figure S8: TDP1-S81E adopts a compact conformation similar to TDP1 wild type. a) Normalized P(r) functions for experimental SAXS curves for TDP1 (red), TDP1 treated with λ phosphatase (green) and TDP1-S81E (blue) indicate a similar conformation of TDP1 and TDP1-S81E (**b**) Comparison of normalized Kratky plots of TDP1 (red), TDP1 treated with λ phosphatase (green), TDP1-S81E (blue) and TDP1-S81A (cyan). Kratky plots show increased unfolding of TDP1-S81A.

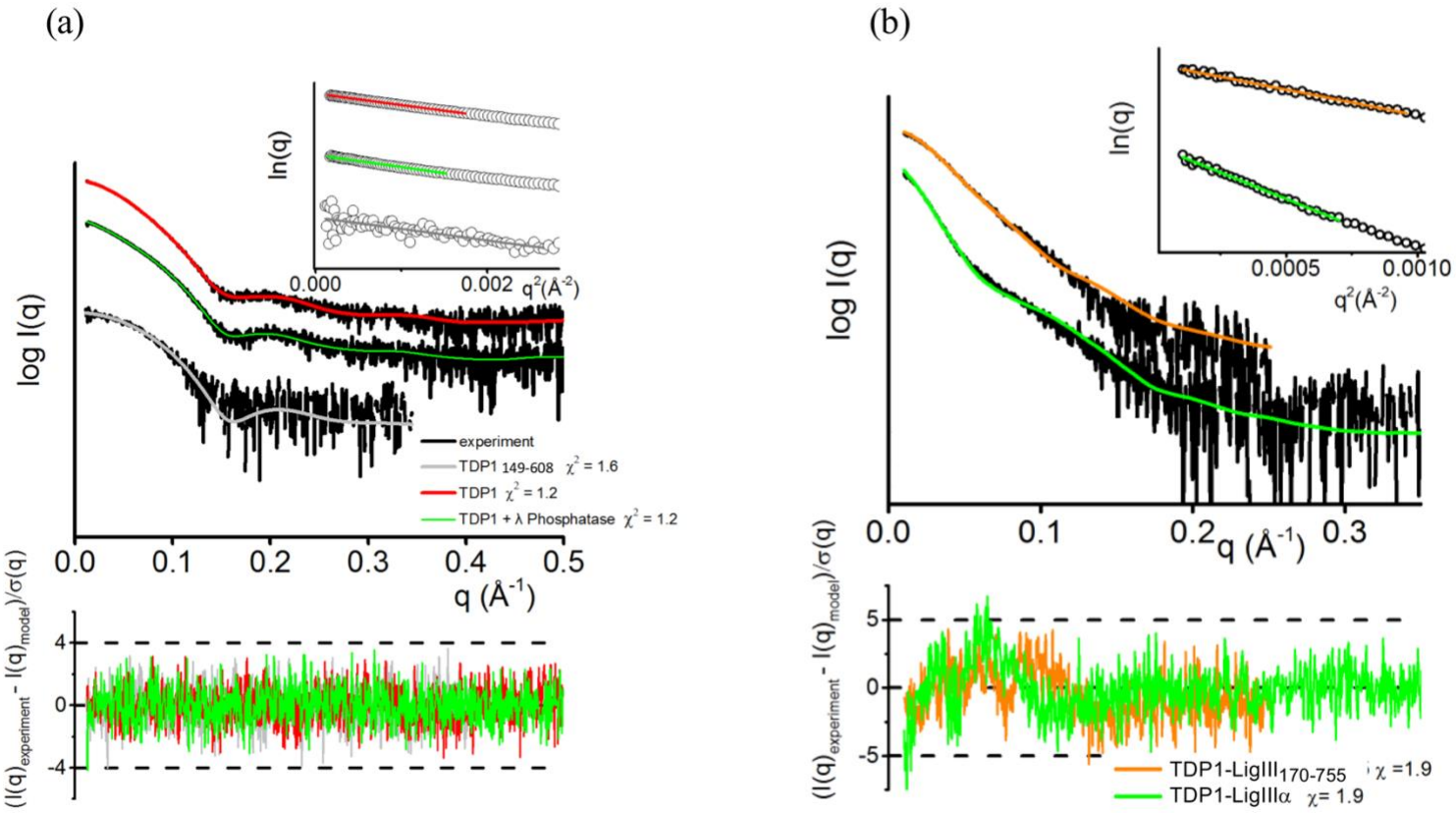

Figure S9: Experimental and theoretical SAXS profiles. (a) Experimental SAXS curves (black) for TDP1, TDP1 treated with λ phosphatase and $TDP1_{149-698}$ are fitted to the theoretical SAXS profiles (colored as indicated) calculated for the atomistic models shown in **Fig. 4c** or the $TDP1_{149-608}$ crystal structure (PDB 1JY1). **(b)** Experimental SAXS curves (black) for $LigIII_{170-755}$-TDP1 and LigIII-TDP1 are fitted to the theoretical SAXS profiles (colored as indicated) calculated for the atomistic models shown in **Fig 6c.** All SAXS fits are shown together with the fit residuals in the lower graph and χ^2 values indicating goodness of fit. Corresponding Guinier plots, with $qR_g<1.5$ are shown in inset.

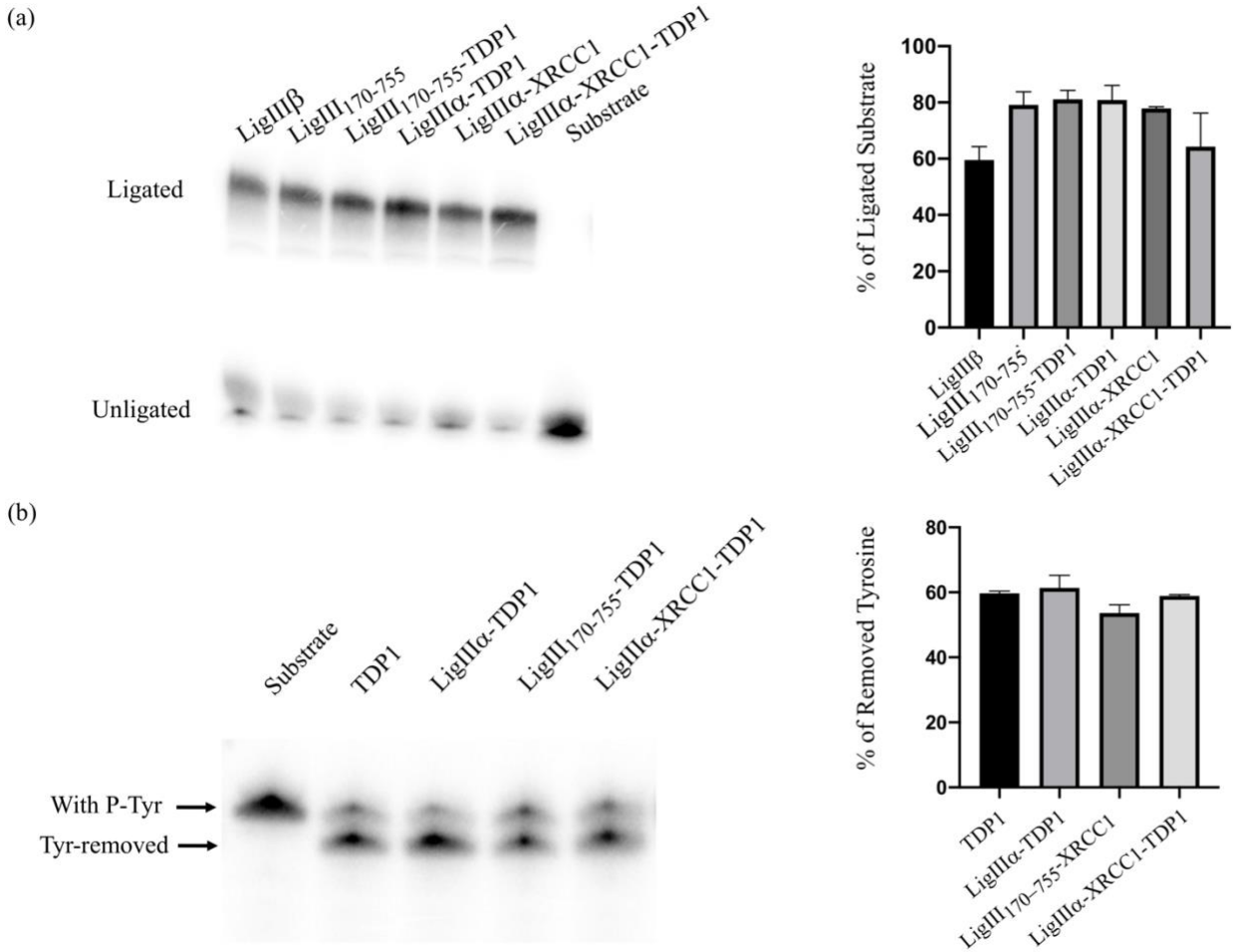

Figure S10: Enzyme activity of purified LigIII associated protein and protein complexes. (a) Ligation activity of purified DNA LigIIIβ, LigIII$_{170\text{-}755}$, LigIII$_{170\text{-}755}$-TDP1, LigIIIα-TDP1, LigIIIα-XRCC1 and LigIIIα-XRCC1-TDP1 (50 fmol of each). Proteins were incubated with a labeled duplex oligonucleotide substrate containing a single ligatable nick substrate (500 fmol) as described in Experimental Procedures. Bar diagram showing % of ligated substrates with standard error of mean calculated from three independent experiments **(b)** Removal of 3'tyrosine from a labeled

duplex oligonucleotide with a 3 ’-phosphotyrosine at a single nick (500 fmol) by TDP1, LigIIIα-TDP1, $LigIII_{170\text{-}755}$TDP1 and LigIIIα-XRCC1-TDP1 (50 fmol of each). Bar diagram showing % of removed tyrosine moiety complexes with standard error of mean calculated from three independent experiments.

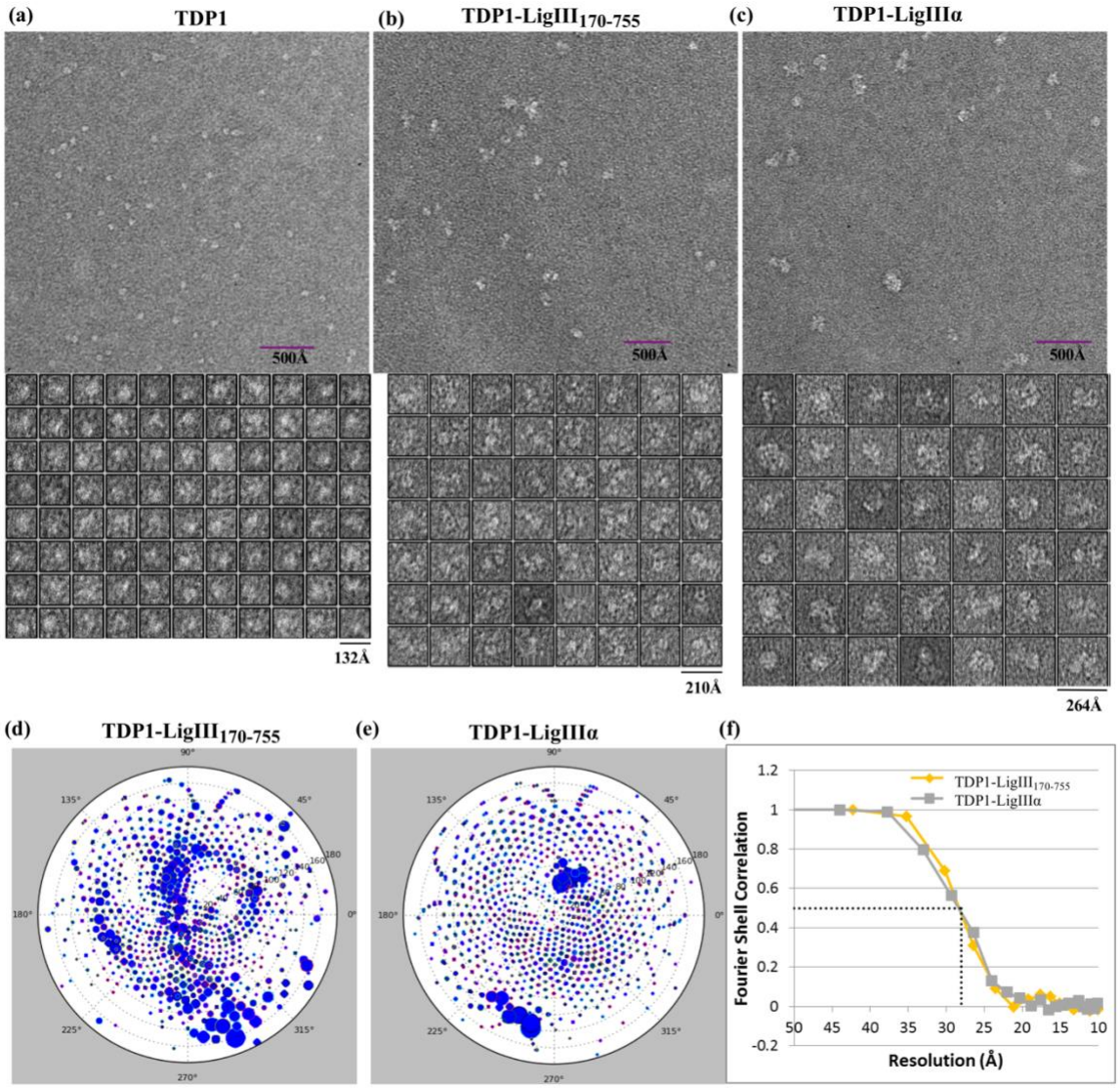
(a)
TDP1
500Å
132Å
(b)
TDP1-LigIII170-755
500Å
210Å
(c)
TDP1-LigIIIα
500Å
264Å
(d)
TDP1-LigIII170-755
(e)
TDP1-LigIIIα
(f)
TDP1-LigIII170-755
TDP1-LigIIIα
Fourier Shell Correlation
Resolution (Å)
1.2
1
0.8
0.6
0.4
0.2
0
-0.2
50
45
40
35
30
25
20
15
10

Figure S11: Raw data and metrics of negative stain EM of TDP1, LigIII$_{170\text{-}755}$-TDP1 and LigIII-TDP1. Representative raw micrographs (upper row) and single particles (middle row) of TDP1 alone **(a)**, and in complex with LigIII$_{170\text{-}755}$ **(b)** or LigIIIα **(c)**. The box sizes of the extracted particles are 132, 210 and 264Å, respectively. Angular distribution of single particles contributing to the TDP1-LigIII$_{170\text{-}755}$ **(d)** and TDP1-LigIIIα **(e)** 3D maps. Fourier shell correlation **(f)** indicates that both maps have a resolution of 28Å using the 0.5 cut-off criterion